Design and Use of PET Tomographs: The Effect Of Slice Spacing

Tom R. Miller, Jerold W. Wallis, and Robert A. Grothe, Jr.

The Edward Mallinckrodt Institute of Radiology, Washington University School of Medicine, St. Louis, Missouri

With modern positron tomographs producing 14, 21, or more transaxial slices, the effects of slice spacing on quantitative reconstruction and three-dimensional displays must be evaluated. This analysis can be approached in terms of the partial volume effect, quantified by the recovery coefficient, or in terms of sampling theory leading to the concept of aliasing. The axial recovery coefficient varies as a function of the position of an object in relation to the slices, with greater variability for larger slice spacings and finer axial resolutions. The aliased image power varies in the same way. The variability in the recovery coefficient and aliasing increase when smaller objects are imaged. Tomographs should be designed with slice spacing approximately half the full-width at half-maximum axial resolution of the tomograph; finer spacing does not appear to confer significant advantages. Thus, quantification and display in positron tomography depend on slice spacing, resolution, and object size.

J Nucl Med 1990; 31:1732–1739

In the early years of positron emission tomography (PET), studies were performed with tomographs that produced a single transaxial slice or, at most, seven slices (*1*). More recently, machines have become available or are under development that can collect studies consisting of 14, 21, or more transaxial slices (*2–5*). Errors in quantification in the transaxial plane caused by imperfect image resolution have been well studied for the case of single-slice data (*6–8*). With the widespread use of multi-slice machines, a further evaluation of these issues with particular attention to the axial or z-axis partial volume effect is warranted. The errors introduced in quantitative analyses and three-dimensional reconstructions caused by the poor sampling of the older machines requires further study, and the number of slices required for accurate PET imaging with the modern machines needs to be determined.

First, the partial volume effect will be analyzed theoretically for both single-slice and multi-slice imaging. An important result of our work is that the partial volume effect varies with respect to the positions of the slices in relation to the imaged objects. This variability is especially pronounced in the axial direction when slice spacing is great. The variability will be shown to be closely related in multi-slice imaging to the signal-processing concept of aliasing. Graphical data will be provided to permit evaluation of any PET tomograph with use of the partial volume and aliasing concepts. Implications for quantitative PET and for generation of three-dimensional displays will be discussed.

Received Oct. 17, 1989; revision accepted Mar. 29, 1990.

For reprints contact: Tom R. Miller, MD, PhD, The Edward Mallinckrodt Institute of Radiology, 510 S. Kingshighway Blvd., St. Louis, MO 63110.

METHODS

Analysis in the Object Domain and the Frequency Domain

The errors introduced in multi-slice PET imaging due to the finite number of slices and the system resolution can be analyzed in the spatial, or object, domain in terms of the familiar concepts of partial volume, recovery coefficient and scatter, or "spillover," fraction (*6–8*). Alternatively, the analysis can be carried out in the spatial-frequency domain where the imaging is considered as a sampling problem, thus, introducing the concept of aliasing caused by undersampling (*9*). The seemingly disparate concepts of variable partial volume effect and aliasing are, in fact, parallel ways of viewing the uncertainty introduced by undersampling. These two approaches provide complementary insights into the problem of sampling in PET tomographs: the concept of the recovery coefficient is most relevant to problems of quantification while the aliasing approach is of greater value in considerations of three-dimensional display because the magnitude of aliasing provides a global measure of the corruption of the acquired image data by undersampling.

Spatial Domain Analysis—The Recovery Coefficient

The recovery coefficient, RC, has been defined as the ratio of the peak detected counts in an object with constant count intensity to its actual count density in the absence of background or other structures (*6,7*). The recovery coefficient used in PET analysis assumes that the detector is centered upon an object with uniform activity. Here, we generalize the concept of the recovery coefficient to include the situation in which the detector is not centered over the object. We define RC(Δx) to be the ratio of the detected counts arising from a constant object to the actual counts when the center of the object is displaced by Δx from the center of the detector. The calculation of RC(Δx) assumes there is no activity outside the object.

object. (The effect of outside activity raising the counts detected in the object is discussed below.)

In an ideal imaging system with perfect spatial resolution, RC(Δx) would be equal to unity or zero, depending upon whether the detector were positioned over the object. In PET imaging, RC(Δx) is dependent upon the total system blurring, characterized by the point-spread function (PSF) as well as the object size. The detected activity, I(x), at any point, x, in the image is the convolution of the PSF with the activity distribution of the object, O(x).

$$I(x) = \int_{-\infty}^{+\infty} O(x')\ PSF\ (x' - x)\ dx' \qquad (1)$$

In Figure 1, O(x) represents a one-dimensional object of length d and constant intensity N. The PSF is modeled as a Gaussian with standard deviation σ (where FWHM = 2.35σ). The value of RC(Δx) for this situation is given by:

$$RC\ (\Delta x) = \frac{I(\Delta x)}{N} = \frac{N \int_{-d/2+\Delta x}^{d/2+\Delta x} PSF\ (x)\ dx}{N}. \qquad (2)$$

Because the recovery coefficient is independent of the object intensity in the absence of background, RC(Δx) can be calculated from the estimate of the object size if Δx is known.

Extension of Equation 2 to a multiple-detector system is quite straightforward and illustrated in Figure 1 for an inter-detector spacing S. The multi-detector recovery coefficient is the maximum value of RC(Δx) among the n detectors:

$$\text{multi-detector } RC(\Delta x) = \max\ (I(\Delta x - nS)/N) = I(\min|\Delta x - nS|)/N. \qquad (3)$$

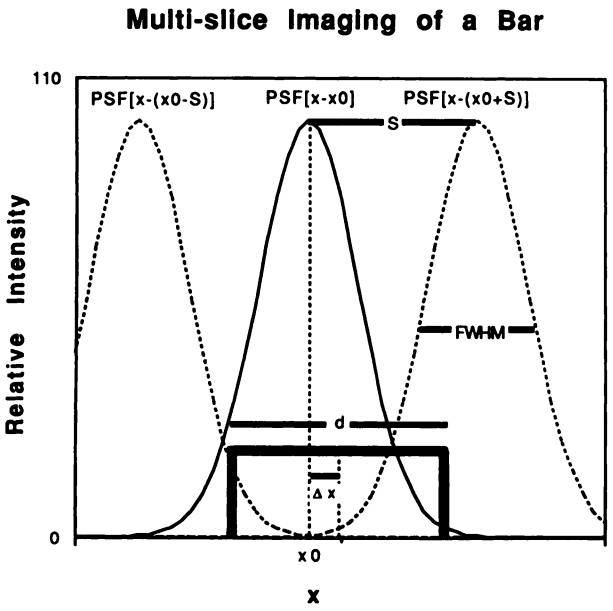

FIGURE 1
The Gaussian blurring function with PSF and FWHM is shown for three slices spaced a distance, S, apart. A bar with uniform activity and diameter, d, is positioned a distance Δx from the center of the middle slice.

For a multi-detector system, RC(Δx) reaches its maximum value when Δx is zero and its minimum value when Δx is S/2. The variability can be assessed by a measure, E_{rc}, defined as the difference between the maximum and minimum values of the recovery coefficient normalized by the maximum value of the recovery coefficient:

$$E_{rc} = \frac{RC_{max} - RC_{min}}{RC_{max}}. \qquad (4)$$

Since the exact axial position, Δx, is typically not known, the appropriate way to deal with this variability is to recognize that the actual recovery coefficient may have any value between its maximum at Δx = 0 (RC_{max}) and its minimum at Δx = S/2 (RC_{min}). Thus, E_{rc} represents this uncertainty in the recovery coefficient. For example, if a 10% maximum uncertainty in the recovery coefficient were judged to be acceptable in an experimental measurement, then $E_{rc} \leq 0.1$ would be an acceptable value. The use of the value RC(Δx = 0) to assess the partial volume effect, as is generally done in PET studies, may lead to dramatically incorrect results when the variability of the recovery coefficient is significant. Substantial variability reflects inadequate sampling.

The same concepts can be extended to three dimensions. The mathematical derivations are more complex but follow directly from the basic equations presented above. The three-dimensional expressions for the spherical activity distributions employed here are presented in detail in the paper by Kessler et al. (8).

Frequency Domain Analysis—Aliasing

Aliasing refers to the generation of artifactual data due to inadequate sampling of a continuous function. Aliasing is best treated in the context of digital signal processing theory employing frequency-domain analysis (9). The partial volume effect is usually analyzed in the object domain and quantified with use of the recovery coefficient, although, as discussed below, the extent of variability of the recovery coefficient in a multi-slice tomograph is linked to aliasing.

The detection and display of an image can be modeled as a series of steps:

1. Blurring of the radioactivity distribution due to the finite range and angular spread of the positrons, scatter in the patient, and detector effects.
2. Sampling of the blurred radioactivity distributions.
3. Interpolation between sampled points to yield a smooth final image.

The effect in the frequency domain of these steps is easily shown graphically, as in Figure 2, where the power (the square of the amplitude of the frequency terms) is shown as a function of spatial frequency. The one-dimensional case will be considered here since the calculations can be easily generalized to three dimensions as discussed above. Consider an object, such as a 10-mm bar, that has been blurred by a Gaussian PSF with FWHM = 10 mm. Sampling of the blurred radioactivity distribution with slice spacing S in the object domain yields a Nyquist frequency f_N = 0.5 S in the frequency domain. The sampling process leads to replication of the power spectrum of the blurred object at every multiple of $2f_N$, as shown in the figure. To combine slices in PET imaging to produce a three-dimensional display, the sampled activity is reconstructed with

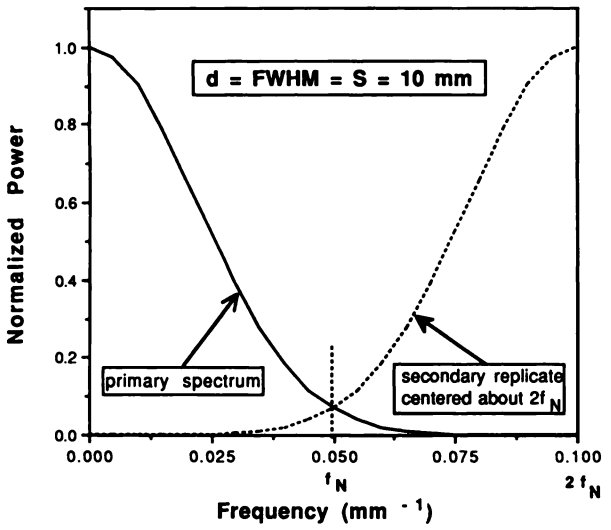

FIGURE 2
The power of a blurred, sampled bar is shown. The primary spectrum is shown along with the replicate due to sampling arising at twice the Nyquist frequency. Note the overlap of this replicate into the primary frequency range below the Nyquist frequency.

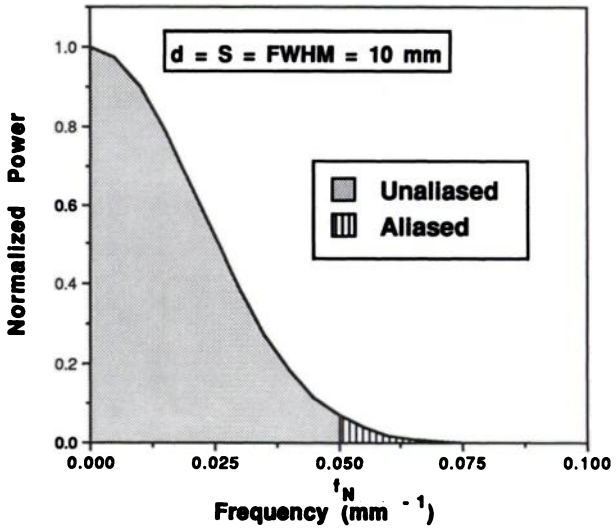

FIGURE 3
The aliased and un-aliased components are shown for the power spectrum of Figure 2.

use of an interpolating filter in the axial direction. This filter can be a square-window function saving all frequencies up to the Nyquist frequency while eliminating higher frequencies, or a spatial-domain linear-interpolation filter, usually employed in PET reconstruction.

The error arising from sampling and reconstruction can be thought of as both the loss of information above the Nyquist frequency and the corruption of the information below the Nyquist by its superposition with artifact-producing "aliased" components from the secondary and higher replicates. The degree of aliasing will depend on the frequency content of the object (related to the object shape), the degree of blurring, and the sampling interval. The magnitude of the aliasing can be assessed for a given object and imaging conditions by considering the power contribution of frequency components above the Nyquist frequency in the blurred image before sampling relative to the total power in the image (Fig. 3). It is this image power above the Nyquist frequency that is folded back, or aliased. An error measured, E_a, can be defined that represents the proportion of the total image power which is aliased:

$$E_a = \frac{\text{power aliased}}{\text{total image power}} = \frac{\int_{f_N}^{\infty} |O(f)\ MTF(f)|^2\ df}{\int_{0}^{\infty} |O(f)\ MTF(f)|^2\ df} \quad (5)$$

Here MTF(f) is the modulation transfer function, the Fourier transform of the PSF, and O(f) is the Fourier transform of the object.

The object-domain concept of the recovery coefficient, presented in the previous section, is mathematically related to the frequency-domain concept of aliasing. This relationship is a consequence of the fact that the object- and frequency-domain representations are a Fourier transform pair (9). While the Fourier integrals representing the recovery coefficient can be written, the mathematics is cumbersome and sheds few insights directly. A better appreciation of the relationship between aliasing and variability in the recovery coefficient is achieved by consideration of their dependencies, as illustrated graphically below. When there is no aliasing ($E_a \approx 0$), the recovery coefficient for a multi-detector system will not change as a function of detector placement ($E_{rc} \approx 0$). The variability of the recovery coefficient correlates with the amount of power aliased, assessed above by the error measures E_{rc} and E_a. Both quantities decrease with closer sample spacing, increased object size, and increased blurring.

Theoretical Calculations

The equations presented above were used to generate a series of graphs of E_{rc} and E_a for typical ranges of parameters for PET tomographs and object sizes.

Experimental Measurements

To validate the theoretical calculations, an experiment was performed with use of SuperPETT IIb, a time-of-flight tomograph, operating in the 7-slice mode. Slice spacing, S, is 14.5 mm and axial resolution is 11 mm FWHM. A plastic sphere with inside diameter of 15 mm was filled with fluorine-18 at a concentration of 80 μCi/cc (3 MBq/cc). After obtaining a transmission scan, the sphere was positioned on the center axis of the tomograph near the center slice. Images were then collected for 5 min. Data collection was repeated as the sphere was advanced in 2-mm increments axially for a total translation of 14 mm. Next, a sphere with diameter 38 mm was filled with fluorine-18 of the same concentration and imaged for 2.5 min at several axial positions. Measurement with this large sphere served to calibrate the sensitivity of the tomograph since the calculated recovery coefficient is very close to unity (0.98–1.00) with only a small variation with position.

The 7-slice data were reconstructed with use of a confidence-weighted algorithm (10) employing a Gaussian filter function in the transaxial plane with FWHM = 10 mm. This filter value is very close to the 11 mm axial blurring of the tomograph, thus insuring an essentially isotropic, three-dimensional blurring function. The reconstruction algorithm incorporates corrections for differences between in-slice and cross-slice sensitivities. After adjustment for radioactive decay, the recovery coefficient was computed according to Equation 3 for each sphere position.

RESULTS

To assess the variability of the recovery coefficient in a multi-slice tomograph, the three-dimensional versions of Equations 2 and 3 were used to compute the recovery coefficient for a sphere as a function of Δx, the position of the sphere in relation to the midpoints of the two nearest slices. Figure 4 shows the three-dimensional recovery coefficients for imaging in SuperPETT IIb in the 7-slice mode. For the sphere with a larger diameter compared to the axial resolution of the tomograph (d = 38 mm, d/FWHM = 3.5) used in the calibration measurements, there is variation of only a few percent with offset, Δx, and the data are not shown. However, for the smaller sphere (d = 15 mm, d/FWHM = 1.4), there is a large variation in the recovery coefficient. The small discrepancy at mid-slice may be related to slight deviation of the axial blurring from a Gaussian shape.

Additional recovery coefficients were computed from Equations 2 and 3 for differing sphere diameters, slice spacings, and system resolutions. Figure 5 shows the effect of slice spacing for SuperPETT IIb when spacing is changed from 14.5 mm (7-slice mode) to 7.25 mm (14-slice mode). Note that the maximum recovery coefficient with the sphere centered on the slice is the same in both cases while the minimum recovery coefficient is much lower with the larger spacing.

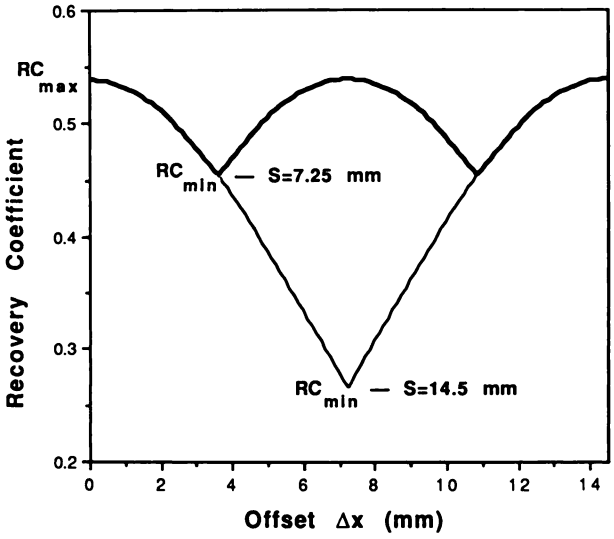

FIGURE 5
The theoretically computed recovery coefficients are shown as a function of offset for the 7-slice imaging situation of Figure 4 (thin line) and for the same tomograph operating in the 14-slice mode where S = 7.25 mm (heavy line). Note that the maximum recovery coefficient (RC_{max}) is the same in both cases while the minimum value (RC_{min}) is much lower when slice spacing is greater (S = 14.5 mm).

While the analysis to this point has focused on the variability in the recovery coefficient, it is also important to emphasize that the magnitude of the recovery coefficient is strongly dependent on object size. Figure 6 shows recovery coefficients for differing sphere sizes

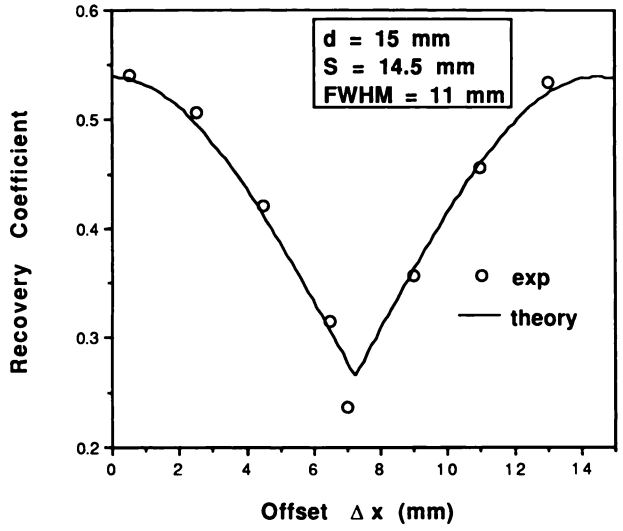

FIGURE 4
The experimentally measured recovery coefficient and the calculated, theoretical value is shown for a sphere with diameter of 15 mm imaged in SuperPETT IIb operating in the 7-slice mode.

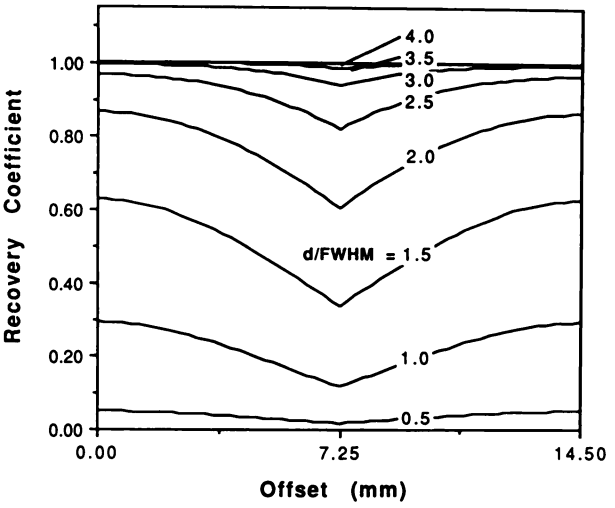

FIGURE 6
Theoretical recovery coefficients are shown for 7-slice imaging in SuperPETT IIb of spheres with diameters d. Sphere sizes are expressed as the ratio d/FWHM where axial resolution = 11 mm. Note the values near unity for imaging of large spheres and more variable recovery coefficients when smaller spheres are imaged.

(expressed as the ratio d/FWHM) for SuperPETT IIb in the 7-slice mode. These graphs show that the recovery coefficient varies with position while, as pointed out previously (*6–8*), it diminishes substantially with smaller objects.

The ratio of the maximum change in the recovery coefficient to the maximum recovery coefficient, E_{rc} (Eq. 4), is shown in Figures 7A-B for fixed rations of d/FWHM and S/FWHM, respectively. The results of the frequency-domain calculations based on Equation 5 are shown in Figures 7C-D for the same fixed rations. The slight ripple and the failure of E_a to go to zero in the aliasing figures is artifactual and arises from use of a simulated sphere with steep edges, leading to ringing in the power spectrum and infinitely-high frequency terms. The data in Figures 7A and 7C are useful in selecting a desirable slice spacing, while Figures 7B and 7D show the effect of axial object size for fixed slice spacings.

The data in Figures 7A–D can readily be used to evaluate any tomograph based on its published specifications. For example, for SuperPETT IIb in the 7-slice mode (S = 14.5 mm, resolution = 11 mm FWHM, S/FWHM = 1.32), quantitative measurements will have an error in the recovery coefficient E_{rc} of 0.31 when an object with axial extent d = 2 FWHM is imaged (Fig. 7A). The error drops to essentially zero for images of a 4–5 cm object (d/FWHM = 3.5–4.5). From Equation 4, the E_{rc} of 0.31 indicates a maximum uncertainty in the recovery coefficient of 31%. Similar inspection of Figure 7C shows a large degree of aliasing for imaging of a small object with negligible error with the 4–5 cm object.

These data assume an isotropic blurring function

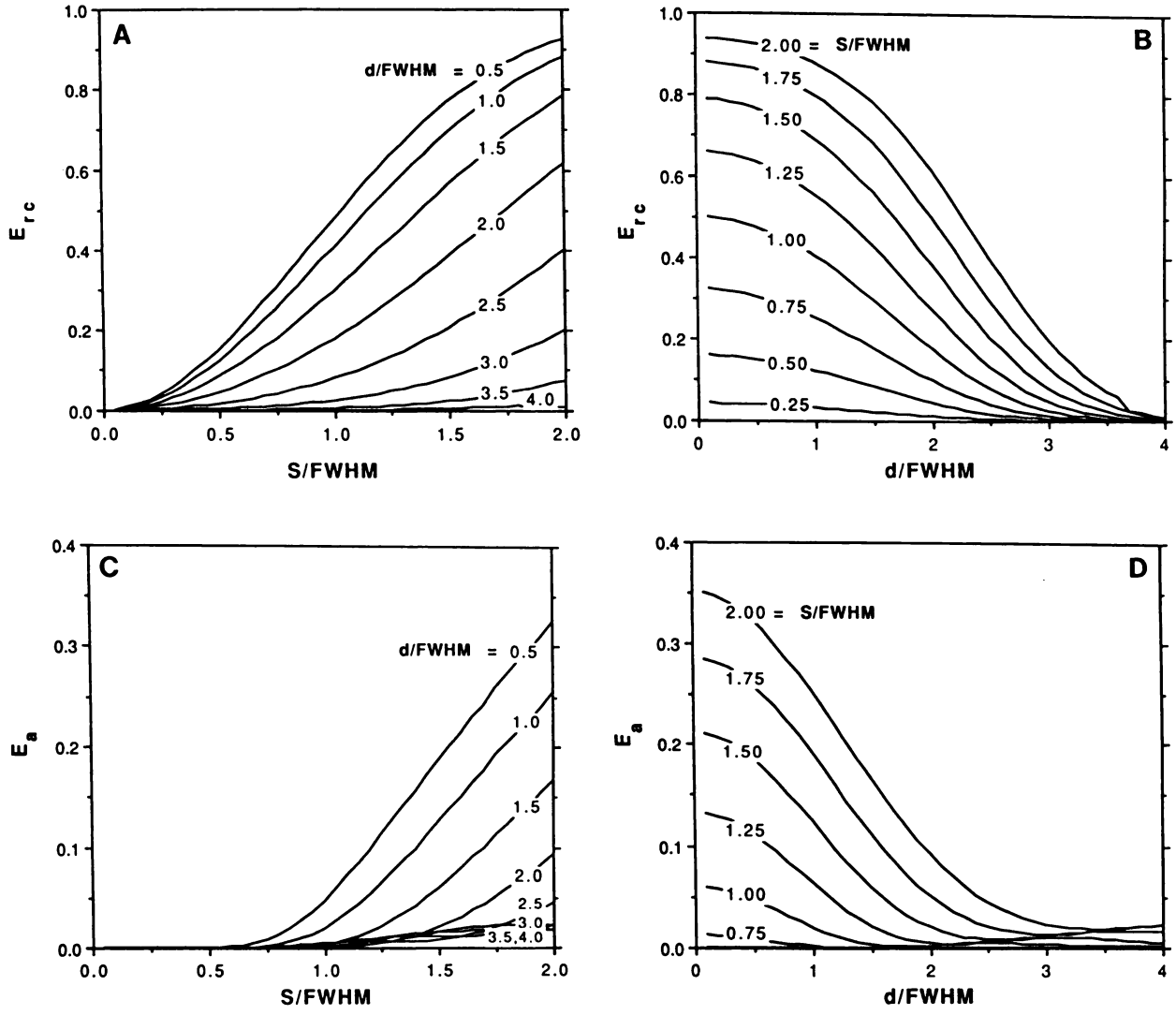

FIGURE 7
The measures of variation in the recovery coefficient, E_{rc}, are shown in panels A and B while aliasing error, E_a, is presented in panels C and D for fixed ratios of sphere diameter-to-resolution (d/FWHM) and of slice spacing-to-resolution (S/FWHM). In the last figure, rations of S/FWHM <0.75 are not shown because the error values are essentially zero.

with equal axial and transaxial resolutions. While the reported transaxial resolution of many tomographs is much better than the axial resolution, in practical, noisy imaging situations the transaxial data are frequently reconstructed with resolution approximately equal to the axial resolution. In any case, use of a sharper resolution in the transaxial plane does not significantly alter the conclusions presented here.

DISCUSSION

In early research in positron tomography, machines were used that produced only a single transaxial slice. Later, tomographs with 4–7 slice capability were developed (*1*). More recently, machines have become available that generate 21 or more closely-spaced transaxial slices (*2–5*). Thus, it is necessary to study the implications of slice spacing on quantitative analysis and three-dimensional display of PET data. A key factor in multi-slice imaging is the partial volume effect. In the early research with single-slice machines, structures were frequently imaged that had a large axial extent, such as experimentally induced myocardial infarcts in dogs. Thus, the partial volume effect in the axial direction could safely be ignored, with attention focused on corrections applied to the data in the transaxial plane. These corrections have been thoroughly evaluated and are quantified in the transaxial plane by the recovery coefficient (*6–8*). For large objects, the loss of counts arises from the blur inherent in the imaging process; the sampling-dependent uncertainty is negligible because of the very fine spacing in the transaxial plane due to the small pixel size employed in image acquisition and reconstruction.

Imaging in multi-slice tomographs of objects with small axial extent or large rates of axial variations raises two important questions: 1) What is the nature of the partial volume effect, quantified by the recovery coefficient, in the axial direction? and 2) How many slices are required in a tomograph to yield quantitatively accurate results and three-dimensional images without significant artifacts? Here we address these two questions, the first by analysis of the axial behavior of the recovery coefficient for realistic imaging situations and the second by use of the recovery coefficient and by a traditional analysis of the effects of undersampling, leading to aliasing in the spatial-frequency domain. The effects of noise, differing straight- and cross-slice sensitivities, and varying off-axis resolution are not included in this analysis since they are not fundamental to the present considerations although they lead to well-known effects on actual images.

In this work, we show that the recovery coefficient varies with the position of the object in relation to the slice (see Equations 2–4 and Figs. 1, 4–6). If the location of the imaged object is known in relation to the slice positions, then an accurate partial volume correction can be applied if the object size and resolution of the imaging system are known. However, if the offset of the object Δx from the slice center is not known, then the recovery coefficient used in quantitative experiments will have an associated uncertainty. This uncertainty will depend upon the axial extent of the object, the slice spacing, and the axial blur of the tomograph (Fig. 7).

An alternative approach to studying the effect of differing slice spacings (related to the number of slices in the tomograph) is by a frequency-domain analysis of sampling that leads to the concept of aliasing. The recovery coefficient approach is most directly applicable to quantification of slice data and is more familiar to practitioners of positron tomography. The aliasing concept is, however, better suited to evaluation of artifacts produced in generation of three-dimensional images (*9, 11*). Three-dimensional algorithms are frequently quite complex, involving interpolation, filtering, ray tracing, and other steps. Thus, a general measure of the degree of corrupted information inherent in the data before digital manipulation is required. Aliased power is such a general measure. Furthermore, considerations of the frequency content of an image, e.g., in Figure 3, is useful in design of digital filters and interpolation functions (*12*). This classical sampling analysis is presented above with results for typical object sizes and PET tomographs (Figs. 7C–D). Since the aliasing power will never be exactly zero and depends on object shape, the acceptable magnitude of aliasing is somewhat subjective. However, infinitesimal aliasing power ($E_a \approx 0$) will never lead to errors while modest amounts of aliasing should be tolerable in real imaging situations since the degrading effects of noise will tend to mask the effects of small amounts of aliasing.

Note that, for a given object, aliasing depends on the blur in the imaging system as well as upon the slice spacing. Thus, in designing a PET tomograph these two parameters should be matched, i.e., a large number of slices giving extremely close spacing is not warranted if axial resolution is poor, and wide spacing is undesirable if resolution is high.

The specific, practical implications of this and earlier work for the design and use of PET tomographs are relatively straightforward. First, the maximum value of the recovery coefficient should be calculated from knowledge of object size and tomograph resolution, as pointed out previously (*6–8*). This recovery coefficient will be less than unity (see Fig. 6). Then, the uncertainty in the recovery coefficient due to axial position, evident in Figure 6, is computed from the data in Figures 7A–B. If a maximum error in the computed recovery coefficient of approximately 10% is deemed to be acceptable then, from Equation 4, $E_{rc} \approx 0.1$. For moderate-size objects (d/FWHM = 1.5–2), Figure 7A then leads to the estimate S/FWHM ≈ 0.5–0.7. Note also that the

graph of E_a (Fig. 7C), begins to rise dramatically from essentially zero for moderate-size objects when S/FWHM $\approx$ 0.75. Thus, for typical objects, the slice spacing of the tomograph should be approximately 50%–75% of the z-axis resolution (FWHM). A closer slice spacing, frequently leading to a more costly machine with more slices, does not confer advantages, while a larger slice spacing (implying fewer slices) can result in significant uncertainty in the recovery coefficient (a large E_{rc}) and substantial aliasing (large E_a). If only objects with large axial extent are imaged, e.g., d/FWHM = 3–4, then a larger slice spacing can be tolerated. In that case, a tomograph with fewer slices will give acceptable results. Thus, tomographs now in use, such as SuperPETT IIb with 14 slices (S/FWHM = 0.66), have adequately close slice spacing for all applications, while the older 7-slice machines, e.g., SuperPETT I, will produce relatively artifact-free data only when imaging objects with known axial extents of several cm.

These considerations assume structures that do not move during data acquisition, such as the brain. For studies of the heart where there is cardiac and respiratory motion, the criteria can be relaxed somewhat because there may be substantial axial motion, leading to blurring of the radioactivity distribution.

The concepts of aliasing and variability of the recovery coefficient seem to be quite unrelated since the conceptual approaches and mathematical expressions are very different. In fact, both concepts provide ways to assess the degree of undersampling, as described in the Methods section; one operating in the spatial domain and the other in the mathematically equivalent frequency domain. The partial volume effect is usually thought of as arising from the blur inherent in imaging. This analysis shows that, for a given object size, the peak value of the recovery coefficient is a function of blur while the variability in the recovery coefficient is directly related to the sampling interval as well as the blur, thus suggesting an aliasing phenomenon. In this sense, the partial volume effect, quantified by the recovery coefficient, is due both to blur and to aliasing.

The paper of Kessler et al. (*8*) pointed out that the recovery coefficient as originally defined must be modified in the presence of background activity, and that the coefficient is different for hot and cold objects. The principle conclusions presented here are based on a situation with no background or spillover. While the mathematics required to handle these additional effects is straightforward, the computations are tedious and lead to many confusing special cases. Addition of background and spillover tends to reduce contrast, thus somewhat relaxing the criteria developed here. We believe consideration of the pure case is best since the analysis leads to the most strict and straightforward conclusions.

The use of the term "partial volume effect" has not been consistent in earlier work. Frequently, usage of the term has tended to follow that of the early literature in computed tomography, referring to a reduction in detected activity due to axial spacing greater than object size. In contrast, loss of detected activity due to blurring in the transaxial plane has been quantified by a "recovery coefficient" that does not consider detector spacing because of the close proximity of the detected elements (pixels) in the transaxial plane (*6–8*). In fact, as was shown in the Methods section, the loss of data due to the axial undersampling (the traditional partial volume effect) is fundamentally the same as the effect in the transaxial plane; in both cases the recovery coefficient is determined by the relationship between the object size and the blur in the imaging system and by the detector spacing. In the transaxial plane, the detector spacing (pixel size) is very small in relation to image blur and, hence, the variability in recovery coefficient is negligible. In contrast, the recovery coefficient may vary significantly in the axial direction due to wide slice spacing. Thus, we prefer to think of the "partial volume effect" as fundamentally a single phenomenon, quantified by the recovery coefficient, in both the axial and transaxial planes. In the axial direction, the recovery coefficient may deviate significantly from its maximum value, which depends only upon blur, and assume lower values when the detected activity is not centered on a slice.

In summary, the relationship between slice spacing, resolution, and object size should be considered when designing or purchasing PET tomographs and when interpreting tomographic data. Failure to appreciate this relationship can lead to significant errors in quantification of PET data and in three-dimensional reconstructions.

ACKNOWLEDGMENTS

This work was supported in part by a grant from Siemens Medical Systems, Inc., Hoffman Estates, IL. We are grateful to Mark A. Mintun, MD for valuable discussions.

REFERENCES

1. Ter-Pogossian M, Ficke DC, Yamamoto M, Hood JT, Super PETT I: a positron emission tomography utilizing photon time-of-flight information. *IEEE Trans Med Imag* 1982; 1:179.
2. Lewellen TK, Bice AN, Harrison RL, Pencke MD, Link JM. Performance measurements of the SP3000/UW time-of-flight positron emission tomograph. *IEEE Trans Nucl Sci* 1988; 35:665–669.
3. Mullani NA, Wong WH, Hartz RK, et al. Design and preliminary results from Posicam: a high resolution positron camera [Abstract]. *J Nucl Med* 1986; 27:973.
4. Muehllehner G, Karp JS, Mankoff DA, Beerbohm D, Ordonez CE. Design and performance of a new positron tomograph. *IEEE Trans Nucl Sci* 1988; 35:670–674.

5. Muehllehner G, Karp JS. Positron emission tomography imaging—technical considerations. *Semin Nucl Med* 1986; 16:35–50.
6. Hoffman EJ, Huang S-C, Phelps ME. Quantitation in positron emission computed tomography: 1. Effect of object size. *J Comput Assist Tomogr* 1979; 3:299–308.
7. Henze E, Huang S-C, Ratib O, Hoffman E, Phelps ME, Schelbert HR. Measurements of regional tissue and blood-pool radiotracer concentrations from serial tomographic images of the heart. *J Nucl Med* 1983; 24:987–996.
8. Kessler RM, Ellis JR, Eden M. Analysis of emission tomographic scan data: limitations imposed by resolution and background. *J Comput Assist Tomogr* 1984; 8:514–522.
9. Castleman KR. *Digital image processing.* Englewood Cliffs, NJ: Prentice-Hall, Inc.; 1979:161–189, 226–249.
10. Snyder DL, Thomas LJ Jr, Ter-Pogossian MM. A mathematical model for positron-emission tomography systems having time-of-flight measurements. *IEEE Trans Nucl Sci* 1981; 28:3575–3583.
11. Miller TR, Starren JB, Grothe RA Jr. Three-dimensional display of positron emission tomography of the heart. *J Nucl Med* 1988; 29:530–537.
12. Miller TR, Sampathkumaran KS, King MA. Rapid digital filtering. *J Nucl Med* 1983; 24:625–628.